



# Confinement of sulfur species into heteroatom-doped, porous carbon container for high areal capacity cathode

Jing Zhang<sup>a</sup>, Caiyin You<sup>a,\*</sup>, Jian Wang<sup>b</sup>, Hong Xu<sup>a</sup>, Chuanzhi Zhu<sup>a</sup>, Shaohua Guo<sup>a</sup>, Weihua Zhang<sup>a</sup>, Rong Yang<sup>c</sup>, Yunhua Xu<sup>a</sup>

<sup>a</sup> School of Materials Science and Engineering, Xi'an University of Technology, Xi'an 710048, PR China

<sup>b</sup> i-Lab, Suzhou Institute of Nano-Tech and Nano-Bionics, Chinese Academy of Sciences, Suzhou, Jiangsu 215123, PR China

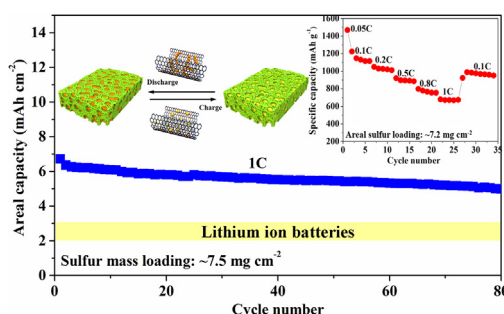
<sup>c</sup> School of Sciences, Xi'an University of Technology, Xi'an 710048, PR China

## HIGHLIGHTS

- A synergistical function was realized through fabricating a polar hierarchical-porous carbon container.
- Polysulfides trapping and electron/ion transfer are simultaneously optimized.
- High areal capacity of  $9.75 \text{ mA h cm}^{-2}$  is achieved under areal sulfur loading of  $7.2 \text{ mg cm}^{-2}$ .

## GRAPHICAL ABSTRACT

Confining sulfur species into polar hierarchical-porous carbon container to achieve high areal capacity based on high sulfur loading.



## ARTICLE INFO

### Keywords:

Lithium-sulfur batteries  
Hierarchical-porous container  
Polar active sites  
High areal capacity  
High mass loading

## ABSTRACT

For the practical application of lithium-sulfur batteries, the high areal capacity based on high loading sulfur cathode is urgently pursued. Herein, the electrochemical rate and cycling performance are significantly enhanced by the design of polar hierarchical-porous carbon container to confine sulfur species. The as-fabricated carbon container shows the following merits: providing an affordable pore volume of  $4.94 \text{ cm}^3 \text{ g}^{-1}$  for confining sulfur and releasing volume changes; facilitating rapid electron/ion transfer pathway; allowing efficient chemisorption of polysulfides by polar active sites synergistically. As a result, the cathode displays a high rate capacity of  $581 \text{ mA h g}^{-1}$  at 8 C and a stable cyclability at 2 C. Importantly, the cathode with  $7.2 \text{ mg cm}^{-2}$  sulfur loading presents a high areal capacity of  $9.75 \text{ mA h cm}^{-2}$  at 0.05 C and high rate performance. Up to  $7.5 \text{ mg cm}^{-2}$ , the high loading cathode could still display a high areal capacity of  $5 \text{ mA h cm}^{-2}$  at 1 C after 80 cycles. Moreover, the container can successfully work in a pouch cell with low E/S ratio. These results show a promising way to promote the practical utilization of Li-S batteries.

## 1. Introduction

Rechargeable lithium-sulfur (Li-S) batteries have been considered as

the highly desirable candidates for electric vehicles and energy storage systems due to their overwhelming theoretical energy density ( $2500 \text{ Wh kg}^{-1}$ ) [1–3]. In spite of the unparalleled merits,

\* Corresponding author.

E-mail address: [caiyinyou@xaut.edu.cn](mailto:caiyinyou@xaut.edu.cn) (C. You).

<https://doi.org/10.1016/j.cej.2019.02.171>

Received 6 December 2018; Received in revised form 21 February 2019; Accepted 23 February 2019

Available online 25 February 2019

1385-8947/© 2019 Elsevier B.V. All rights reserved.

commercialization of Li-S batteries is still hindered by several challenges such as the insulating nature of active materials, the repeated shuttling of polysulfides and the severe volume change during cycling, which become more serious upon application [4–9]. Moreover, to get a comparable energy density with the commercial lithium ion batteries, a sulfur mass loading above  $4 \text{ mg cm}^{-2}$  corresponding to areal capacity higher than  $4 \text{ mA h cm}^{-2}$  is necessary [10–13]. Apart from these, some other minor challenges such as deleterious side reactions in the cells i.e. gas evolution is worthy to be investigated [14].

In the past decades, diverse efforts have been made to address the aforementioned problems through designing the conductive carbon framework or nanostructured polar inorganic compounds [15–28]. Up to now, it is well accepted that carbon hosts are the most promising conductive framework for cathode fabrication [29–36]. Various carbon hosts have been introduced to explore their potential in preparation of cathode with high mass sulfur loading [11,37–42]. However, the reported high areal capacity and cycle life are still very challenging since the cathodes with high areal sulfur mass loading is not effective enough to fulfill the demand of high areal capacity and high energy density. In most cases, the areal loading of sulfur in the majority of the cathodes was far below the application requirement, due to the large specific surface areas mainly originating from the external surface of the nanocomposites rather than the internal porous structure [11,37,40–42]. As the increase of sulfur content in the cathode, the sulfur is likely to stack and wrap a thick layer on the surface of the hosts resulting in the unsatisfactory ionic and electrical conductivity. What's worse, the generated polysulfides may dissolve and randomly redeposit onto the cathode surface to form a passivation layer, bringing about depressed reaction kinetics and high polarization. Moreover, the higher focused stress from large volume expansion would degrade structural integrity of the cathode. Carbon host with large pore volume and hierarchical-porous construction is more desirable for rapid electron/ion transfer and stress releasing [3,10,43–45].

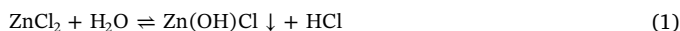
Besides the structural design, the affluent polar sites in the host may also serve as a synergetic confinement effect for the lithium polysulfides and sulfides [24]. Surface chemistry modification (O, N, S or B doping) on the nanocarbon host has displayed significant potential in realization of polar sites for polysulfides confinement [11,37,46–52]. However, in this way, it is evitable to sacrifice the pore morphology for elemental doping. Taking all into consideration, a multi-functional nanocarbon host with large pore volume, hierarchical-pores and polar active sites for synergistically confining sulfur species is of great importance to realize high areal capacity, especially for high mass loading sulfur cathode.

Herein, we have managed to prepare a polar hierarchical-porous carbon container (named as PHPCC) with appropriate pore volume containing hierarchical pores and well-optimized S, N polar sites for synergetic confinement of sulfur species. Benefiting from large pore volume for loading sulfur, hierarchical pores for fast electron/ion transfer and polar elemental doping for strong chemisorption, the cathode with 78 wt% sulfur content exhibits high rate capability of  $581 \text{ mA h g}^{-1}$  at 8 C, and low capacity decay rate of 0.08% per cycle at 2 C within 400 cycles, which is rarely achieved in the previous reports of Li-S cathodes with nano-porous matrices [16,21,24,53]. More importantly, it presents a high areal capacity of  $9.75 \text{ mA h cm}^{-2}$  at 0.05 C under the high sulfur loading up to  $7.2 \text{ mg cm}^{-2}$  and high reversible areal capacity of  $5.0 \text{ mA h cm}^{-2}$  after 80 cycles at 1 C with sulfur loading of  $7.5 \text{ mg cm}^{-2}$ . Our work demonstrates a way of achieving the high areal capacity for the high mass loading cathode through synergistically confining sulfur into the PHPCC, showing the significantly practical potential in realizing high energy density Li-S batteries.

## 2. Experimental

### 2.1. Preparation of polar hierarchical-porous carbon container

There are two typical processes for fabricating the heteroatom-doped hierarchical-porous carbon. Firstly, the mesoporous carbon (MPC) was prepared through a hard template method [54]. Firstly, 3.32 g resorcinol (Aladdin) was dissolved into 5 mL formaldehyde solution (Aladdin), followed by gradually adding 17.3 mL commercial colloidal silica solution (Sigma-Aldrich) and 0.7 mL methyl alcohol under magnetic stirring. Then, the mixture was magnetically stirred for 2 h and cured for 24 h before carbonization in an argon atmosphere at  $900^\circ\text{C}$  for 3 h. The silica nanoparticles were removed by 30 wt% hydrofluoric acid solution. The mixture was repeatedly washed by water and subsequently dried at  $80^\circ\text{C}$  overnight. Secondly, the MPC of 150 mg was dispersed into 160 mL deionized water; 150 mg zinc chloride and 200 mg thiocarbamide were added. The mixture was then sonicated for 1 h to yield a homogeneous blend, and then transferred into 100 mL teflon liner of stainless-steel autoclave. The sealed liner was placed in a pre-heated oven at  $180^\circ\text{C}$  for 8 h. The resultant solid product was collected by filtration and later dried for 12 h. The polar hierarchical-porous carbon container (PHPCC) was finally obtained after evaporating residual zinc at  $800^\circ\text{C}$  for 2 h. To fabricate the hierarchical pores, zinc chloride ( $\text{ZnCl}_2$ ) is added in the hydrothermal process, serving as a pore-forming agent to generate much more pores.  $\text{ZnCl}_2$  is a typical type of pore template used for the activation of carbon [55]. The  $\text{ZnCl}_2$  experiences a hydrolysis firstly and then decomposes to ZnO. Then ZnO nanoparticles could be reduced and evaporated from the carbon leaving the corresponding mesopores:



With the addition of  $\text{ZnCl}_2$ , the PHPCC can experience a second porosity development to get more pores and also maintain the inter-connecting pores along the channel of Zn evaporating, to some extent avoiding the formation of closed pores.

### 2.2. Analysis of polysulfides adsorption

The polysulfides solution ( $0.2 \text{ mol L}^{-1}$ ) was prepared through dissolving 92 mg lithium sulfide and 448 mg sublimed sulfur into 10 mL mixed solvent of DME/DOL (1:1 in volume) at the same time with continuous stirring. Then, the MPC and PHPCC with same mass were soaked into the homogeneous solution (diluted to  $5 \text{ mmol L}^{-1}$ ) for 8 h, respectively. The residual  $\text{Li}_2\text{S}_8$  solutions in the supernatants were collected through filtration. The obtained solutions were diluted by two times with DME/DOL solvent to enable ultraviolet visible (UV-vis) measurements. All the operation was carried out in an Ar-filled glove box.

### 2.3. Preparation of polar hierarchical-porous carbon container-sulfur composites

0.72 g sublimed sulfur (Aladdin, > 99.95%) was added into a solution containing 1.82 g  $\text{Na}_2\text{S} \cdot 9\text{H}_2\text{O}$  and 25 mL deionized water, followed by stirring at room temperature to obtain homogeneous  $\text{Na}_2\text{S}_x$  solution. The as-synthesized PHPCC were dispersed into deionized water by means of sonication. Then, 21 mL  $\text{Na}_2\text{S}_x$  solution was dripped into the aforementioned carbon suspension slowly with strong magnetic stirring. Afterwards,  $2 \text{ mol L}^{-1}$   $\text{HCOOH}$  solutions was added dropwise to the suspension containing PHPCC and  $\text{Na}_2\text{S}_x$  mixture for in-situ deposition of elemental S under overnight continuous stirring. The as-deposited mixture was filtrated and washed by deionized water for many times to remove the soluble impurities. The collection was dried at  $60^\circ\text{C}$  for 24 h, and finally sealed in a vessel full of argon gas. The

vessel was heated at 155 °C for 12 h to obtain PHPCC@S composite. The MPC@S composite was prepared by the same method.

#### 2.4. Preparation of coin cells

The carbon (MPC or PHPCC)-sulfur composite with Super P and polyvinylidene fluoride (PVDF) binder was dispersed in N-methyl-2-pyrrolidone (NMP) solution according to a weight ratio of 7:2:1 under vigorous stirring to obtain homogenous slurry. The slurry was drop cast onto an aluminum foil or thin Ni foam to prepare the cathodes with a controlling sulfur loading of  $\sim 1.2 \text{ mg cm}^{-2}$  to  $\sim 7.5 \text{ mg cm}^{-2}$ . The cathodes were vacuum dried at 55 °C for 48 h before use. Coin cells (LIR2032) were assembled from the fabricated cathode film (circular disks of  $\phi 11 \text{ mm}$ ) with lithium foil as the anode separated by polypropylene membrane separator (Celgard 2400). The electrolyte (Suzhou China) comprises  $1 \text{ mol L}^{-1}$  LiTFSI and 1 wt%  $\text{LiNO}_3$  in 1,3-dioxolane/1,2-dimethoxyethane solution (DOL/DME, 1:1 in volume). The electrolyte/sulfur (E/S) ratio is about  $26 \mu\text{L mg}^{-1}$  per coin cell. The cell was assembled inside a glove box full of high pure argon gas ( $\text{H}_2\text{O} \leq 0.5 \text{ ppm}$ ,  $\text{O}_2 \leq 0.5 \text{ ppm}$ , MBRAUN LABSTAR).

#### 2.5. Materials and cells characterization

The X-ray diffraction (XRD) was collected on an XRD-7000S X-ray diffractometer with Cu-K $\alpha$  radiation ( $\lambda = 0.15418 \text{ nm}$ ) in a  $2\theta$  range from  $10^\circ$  to  $80^\circ$ . X-ray photoelectron spectra (XPS) were obtained from an AXIS ULTRA system. Raman spectra were recorded on a Horiba Laser Raman spectrometer (EUROVECTOR EA3000). Nitrogen absorption and desorption experiment was performed on ASAP 2020 (Micromeritics). Thermal gravimetric analysis (TGA) was conducted on a TG/DTA 6200 setup with a heating rate of  $10^\circ\text{C min}^{-1}$  under nitrogen flow. Scanning electron microscopy (SEM) observation and energy dispersive spectra (EDS) elemental mapping were carried out using a Germany MERLIN Compact Scanning Electron Microscope (Zeiss). Transmission electron microscopy (TEM) samples were imaged using a Tecnai G2 F20 S-TWIN Transmission Electron Microscope. Electrochemical measurements of the cells were carried out on a Neware battery testing system (BTS-5 V 20 mA) within the voltage window of 1.6–2.8 V at different current rates. The electrochemical impedance spectroscopy (EIS) and cyclic voltammetry (CV) were performed with a VMP-3 potentiostat/galvanostat station (Germany).

### 3. Results and discussion

The specific fabrication procedures of the polar hierarchical-porous carbon container (PHPCC) are illustrated in Fig. 1: a) Resorcinol and formaldehyde solution is polymerized together with silica nanoparticles as hard templates to form carbon source and porous structure; b) Then mesoporous carbon (MPC) is obtained after carbonizing and removing template. And the polar sites and increased pore volumes are simultaneously achieved through the following hydrothermal reaction with thiocarbamide and zinc chloride. During this process, zinc chloride serves as a pore-forming reagent to prohibit the partial blocking of pores; c) Sulfur is confined into the PHPCC under capillary force at 155 °C to get homogeneous composite. As revealed in Fig. 1d, the generated polysulfides in cycling are confined by synergetic effect of the hierarchical-porous carbon with large pore volume and polar elemental sites. Meanwhile, the hierarchical-porous structure enables excellent electrolyte immersion for better lithium ions transfer and effective strain releasing [3,23,43,45]. These merits will be confirmed later through electrochemical impedance spectra (EIS) and polysulfide absorption analyses.

Fig. 2a displays the nitrogen absorption/desorption isotherms. The typical nitrogen adsorption/desorption isotherm with a type- $\text{H}_2$  hysteresis loop confirms the presence of mesoporous structure in the MPC and PHPCC [46,48,54]. The PHPCC exhibits a higher surface area of

$1420 \text{ m}^2 \text{ g}^{-1}$  and a larger pore volume of  $4.94 \text{ cm}^3 \text{ g}^{-1}$  than the values ( $649.71 \text{ m}^2 \text{ g}^{-1}$ ,  $2.89 \text{ cm}^3 \text{ g}^{-1}$ ) of the pristine MPC (Table S1). As we all know, the large surface area is able to provide more chances for uniform distribution of S/ $\text{Li}_2\text{S}$  without sacrificing the whole conductivity, ensuring a well dispersion of final discharge product  $\text{Li}_2\text{S}$ . And large pore volume is still a crucial factor for effective sulfur confining and volume accommodation. The pore-size distribution curves derived from Barrett-Joyner-Halenda (Fig. 2b) reveals the hierarchical-porous structure of the PHPCC. The larger mesopores around 20–60 nm can promise sufficient confinement of sulfur and volume change [3,48]. Also, the retained smaller mesopores ranging from 3 to 6 nm are able to promote electrolyte immersion throughout the cathode benefiting a fast Li ions transfer, and release the strain originated from the volume change at the same time [3,23,43,45].

For a better understanding of the pore morphology, the scanning electron microscopy (SEM) and transmission electron microscopy (TEM) were carried out. As can be seen from Fig. 2c, the PHPCC has a morphology feature of disordered porous structure with larger mesopores (20–60 nm, marked by red curves). However, the MPC only shows smaller scales of mesopores with more compact structure (Fig. S1). Through sulfur impregnation process, the PHPCC@S composite still maintains the porous morphology (20–60 nm, marked by red curves) without any bulk sulfur island on the surface (Fig. 2d). In addition, the TEM characterization provides a further observation on the hierarchical-pores. The PHPCC (Fig. 2e) clearly shows the large mesopores (20–60 nm) and small mesopores (3–6 nm) of the hierarchical pores, as marked by the red and blue curves, respectively. The PHPCC@S (Fig. 2f) still maintains the original morphology of hierarchical pores as the PHPCC. This morphology characteristic is in good consistency with the pore-size distribution curves.

The polar chemical doping sites were identified through Raman spectroscopy analysis since it could be considered as the structural defects of the carbon lattices. As shown in Fig. 3a, two remarkable peaks for each sample are clearly observed at approximately 1330 and  $1600 \text{ cm}^{-1}$ , corresponding to D and G band of carbon atom vibration, respectively. The intensity ratio of D band to G band ( $I_D/I_G$ ) has widely been recognized as a parameter to evaluate the degree of defects in carbon materials [46,48]. The PHPCC has a larger  $I_D/I_G$  value (1.44) than MPC (1.21). This suggests the successful introduction of more defect sites in the carbon lattices created by N and S doping (Fig. 3a). The Raman shifts toward the low wavenumber also indicate the implantation of S, N polar sites into the carbon frame [56].

The X-ray photoelectron spectroscopy (XPS) was carried out to analyze the surface chemistry of PHPCC, as shown in Fig. 3b–d, which is another direct proof of N and S polar sites on the PHPCC. The high-resolution view of the strong  $\text{C}_{1s}$  peak in PHPCC (Fig. 3b) shows C–C bond at 284.5 eV, and the peaks at 286.5 eV and 285.2 eV corresponding to C–N–C and C–S bonds, respectively. While in the MPC sample (Fig. S2), the binding peaks of C–N–C and C–S bonds are absent (Fig. S2b). These further prove the successful doping of N and S into carbon lattices. The doping environment of N is also recognized from the high-resolution  $\text{N}_{1s}$  spectrum (Fig. 3c), exhibiting three component peaks of pyridinic N (399.13 eV), pyrrolic N (400.06 eV), and graphitic N (401.65 eV). It is proved that the two dominant types of pyridinic N and pyrrolic N are favorable for chemisorption of polysulfides [45,47]. Two components positioned at 164.10 eV and 165.29 eV can be assigned to C–S–C, C=S bonds in high-resolution spectrum of  $\text{S}_{2p}$  (Fig. 3d), respectively [45,47]. It is evaluated that the overall doping content of the two elements reaches 4.25 at% (3.11 at% for N element and 1.14 at% for S element). This doping amount may provide a certain concentration of polar sites for effective chemisorption of polysulfides.

The successful confinement of sulfur in the above carbon matrices (named as MPC@S and PHPCC@S) were confirmed through X-ray diffraction (XRD), as demonstrated in Fig. 4a. The carbon samples present amorphous nature since the characteristic reflection peaks at  $24^\circ$  and

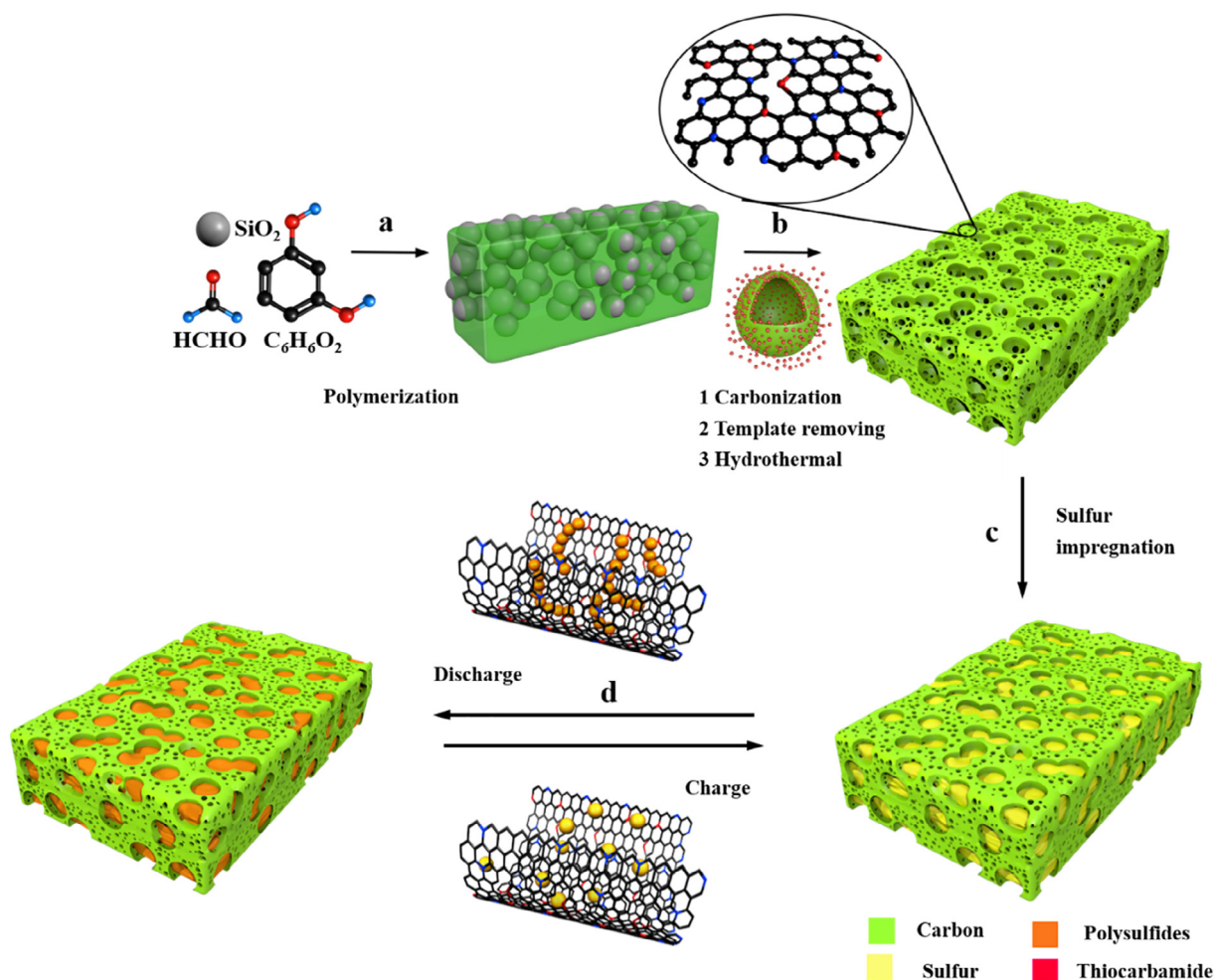


**Fig. 1.** The schematic synthesis process of PHPCC: a) Polymerization and curing; b) Carbonization, template removing and hydrothermal reaction for heteroatom-doping and volume expanding; c) Sulfur impregnation; d) Polysulfides trapping and volume accommodation during electrochemical process.

$44^\circ$  have been replaced by the wide and broad diffraction peaks. After sulfur embedding, the XRD pattern of the MPC@S composite mainly presents the reflection peaks of carbon with some weak peaks of elemental sulfur. While the peaks intensity related to the elemental sulfur become much weaker after doping S and N, as shown in the pattern of PHPCC@S (Fig. 4a). The sulfur weight content of the PHPCC@S composites was evaluated by thermogravimetric analysis (TGA), and the sulfur contents were up to 78 wt% (Fig. 4b). In reality, the PHPCC framework presents a potential of 91 wt% sulfur confinement (Table S2) theoretically. Our work presents the largest potential of confining the high amount of sulfur in comparison with the values of the nanocomposite carbon frameworks reported previously (Table S2) [11,37,45,46,53,57]. Therefore, it can be deduced that the sulfur is well embedded in the porous carbon shells and some un-confined pores could play a role in releasing the volumetric stress during electrochemical process. These also explain the weak XRD diffraction intensity of sulfur (Fig. 4a). The homogeneity of the PHPCC@S composites was further confirmed from the energy-dispersive X-ray spectroscopy (EDS) elemental mappings. The S and N elements (Fig. S3a–d) are homogeneously distributed within the composites in terms of their identically contrast color with C. This implies that the sulfur was evenly confined into the pores of the PHPCC.

To demonstrate the advantages of synergetic effect of porous container on stabilizing the sulfur species, the cells based on MPC@S and PHPCC@S composites were fabricated. Cyclic voltammetry (CV) measurement on PHPCC@S cathode was performed within the potential window 1.6–2.8 V (vs.  $\text{Li}/\text{Li}^+$ ) to identify the electrochemical reactions.

The first five CV curves of the cathode is illustrated in Fig. 5a, which displays two discriminative reduction peaks around 2.29 and 2.07 V, revealing the typical sulfur cathode reduction behavior. The peak at 2.29 V during the cathodic scan is attributed to the conversion from elemental sulfur to long-chain polysulfides ( $\text{Li}_2\text{S}_n$ ,  $4 \leq n \leq 8$ ); and the sharper peak at 2.07 V is related to the further reduction of long-chain polysulfides to insoluble lithium sulfides ( $\text{Li}_2\text{S}_2/\text{Li}_2\text{S}$ ). In the anodic scan, there is a strong peak around 2.32 V with a small shoulder peak at 2.36 V, which can be assigned to the oxidation of lower-order polysulfides ( $\text{Li}_2\text{S}_2/\text{Li}_2\text{S}$ ) to higher-order polysulfides ( $\text{Li}_2\text{S}_n$ ,  $4 \leq n \leq 8$ ) and eventually to sulfur, respectively. And the feature of oxidation peak with a shoulder can remain an excellent repeatability during the five cycles, indicating reversibility of the cathode. An excellent repeatability of the CV curves is detected, indicating a high electrochemical reversibility and stability of the PHPCC@S cathode.

The rate capacities of the two cathodes with sulfur loading of  $\sim 1.2 \text{ mg cm}^{-2}$  were carried out from 0.1 C to 8 C, and the comparison result is shown in Fig. 5b. In contrast to the MPC@S cathode, the PHPCC@S cathode exhibits the superior rate performance up to 8 C. It delivers an initial discharge specific capacity of  $1233 \text{ mA h g}^{-1}$  at 0.1 C ( $1\text{C} = 1675 \text{ mA g}^{-1}$ ), much higher than the controlled MPC@S cathode ( $966 \text{ mA h g}^{-1}$ ). As the increase of current rate, the specific capacity decreases gradually. They are 1016, 892, 818, 748, 681, 634, and  $581 \text{ mA h g}^{-1}$  at 0.2 C, 0.5 C, 1 C, 2 C, 4 C, 6 C and 8 C, respectively. The cathode still has a reversible capacity of  $921 \text{ mA h g}^{-1}$  as soon as the battery cycled backed to 0.2 C, demonstrating an excellent rate performance of the cathode. Such a high rate capacity is very competitive



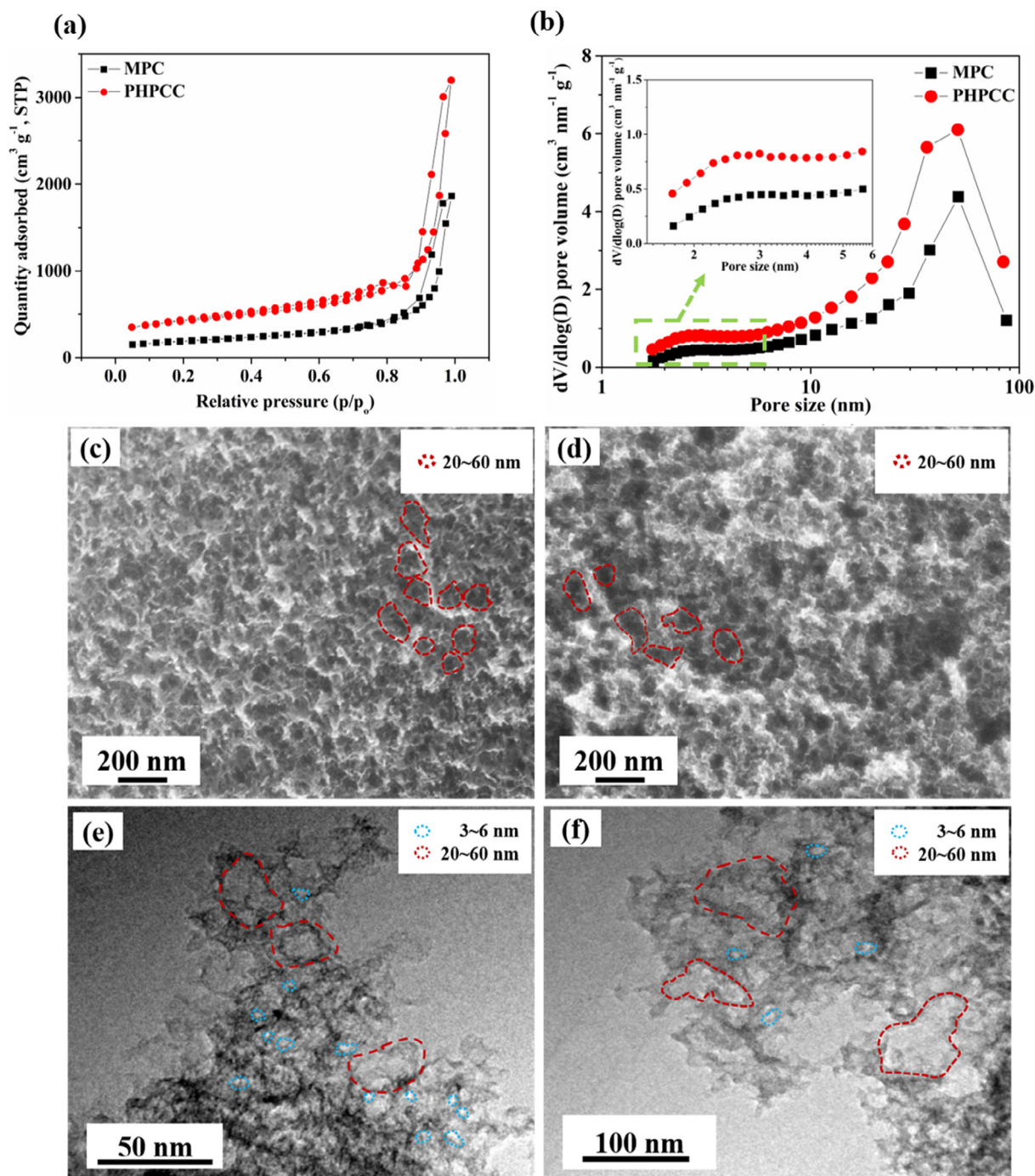


**Fig. 2.** (a) Nitrogen absorption/desorption isotherms and (b) Pore size distribution of MPC and PHPCC and the inset of the high resolution at the micropores and small mesopores range; SEM images of (c) PHPCC and (d) PHPCC@S; TEM images of (e) PHPCC and (f) PHPCC@S. Note: the marked contours schematically indicate representatives of the large mesopores and small mesopores.

with the most previous works with nanocomposite matrixes [16,21,24,53]. In strong contrast, the MPC@S cathode shows degraded performance as it only delivers 471 mA h g<sup>-1</sup> at 6 C and much lower capacity of 377 mA h g<sup>-1</sup> at 8 C. The much-improved rate performance of the PHPCC@S cathode indicates the critical role of the synergetic effect between the large pore volume containing hierarchical-pores and strong chemisorption by polar sites. This featured structure can tightly absorb the polysulfides and largely accommodate the volume variation to maintain the integrity and stability of the cathode under the rapid change of current density. Two distinguished discharge plateaus and two charge plateaus are observed in each specific capacity-voltage profile of the galvanostatic charge-discharge profiles of PHPCC@S

cathode (Fig. 5c), agreeing well with the oxidative and reductive peaks of the CV curves (Fig. 5a). Moreover, almost similar shape of these plateaus is maintained, and the curve still presents an apparent discharge plateau at 1.83 V even at the high current rate of 8 C. As a comparison, the MPC@S cathode displays much lower discharge plateaus at each current rate (Fig. S4), which displays higher electrochemical polarization (polarization potential,  $\Delta E$  [53,56]).

The MPC@S, and PHPCC@S cathodes with sulfur loading of  $\sim 1.2$  mg cm<sup>-2</sup> were cycled at a current rate of 1 C (Fig. 5d). The PHPCC@S cathode shows the superior cycling performance with a high initial capacity of 914 mA h g<sup>-1</sup> while that of the MPC@S is as low as 720 mA h g<sup>-1</sup>, the PHPCC@S cathode experiences slow capacity

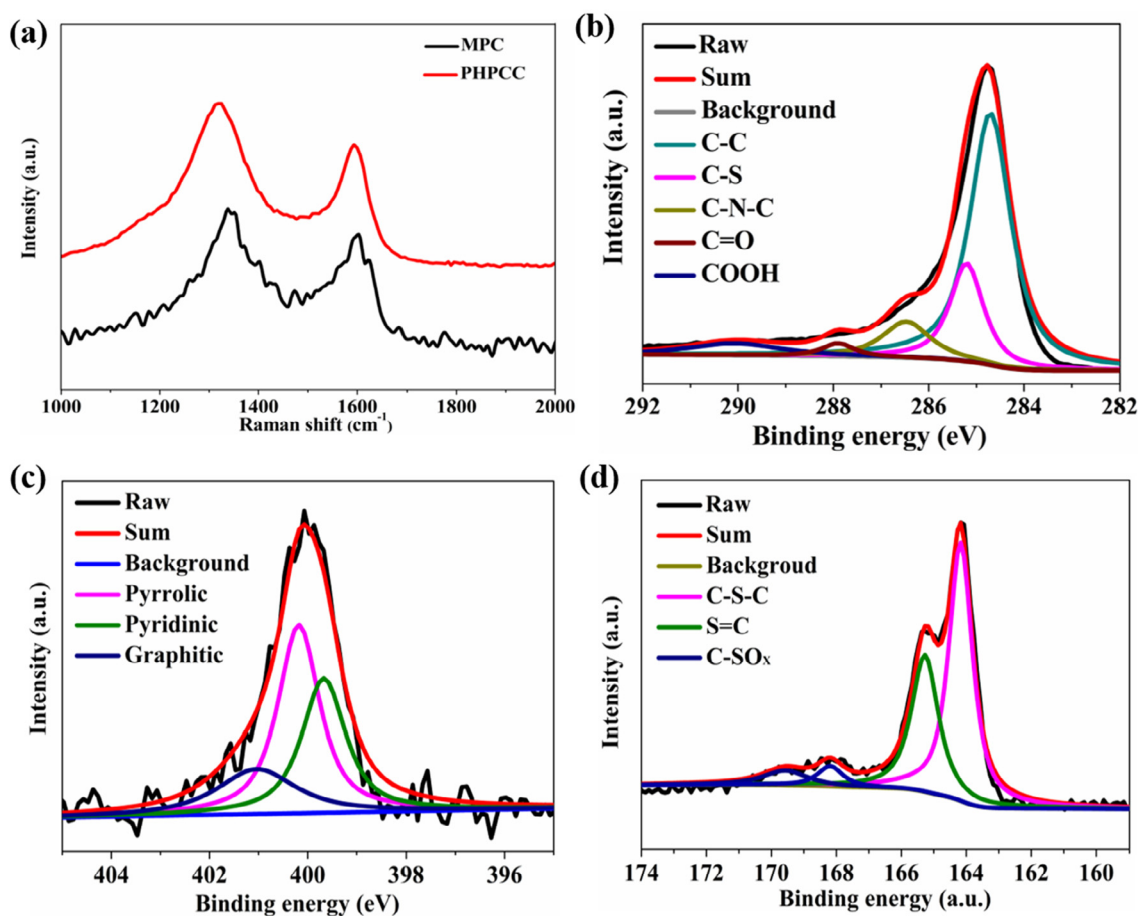


Fig. 3. (a) Raman spectra of MPC and PHPCC; High-resolution spectra of (b) C<sub>1s</sub>, (c) N<sub>1s</sub> and (d) S<sub>2p</sub> of PHPCC.

degradation and can still deliver a higher discharge capacity (829 vs. 584 mA h g<sup>-1</sup>) and retention rate (91% vs. 81%) than MPC@S cathode after 100 cycles. Fig. S5a displays that the discharge capacity of the PHPCC cathode is stabilized around 30 mA h g<sup>-1</sup> at 1 C, suggesting a negligible contribution of the doped sulfur to the total capacity. A series of contrast experiments (Fig. S5b and c) were carried out by varying the amount of silica template and dopant thiocarbamide, respectively, to determine the optimal PHPCC@S cathode. And the cells based on PHPCC@S cathode was also measured using the ether electrolyte without LiNO<sub>3</sub> additive (Fig. S6) for a better confirmation of the synergistic effect.

The detailed advantages of PHPCC framework can be further

clarified from the EIS and the polysulfides adsorption analyses, as presented in Fig. 5e and f. All of the plots are composed of a depressed semicircle within the high-frequency region, corresponding to the charge-transfer process, and a sloping straight line in the low-frequency region corresponding to a semi-infinite Warburg diffusion process (EIS, Fig. 5e). The diameter of the semicircle can be attributed to the charge transfer resistance (*R<sub>ct</sub>*) at interface, which is a measure of the charge transfer kinetics [54]. As shown in Fig. 5e, the PHPCC@S cathode displays a lower *R<sub>ct</sub>* than the MPC@S cathode, demonstrating a faster transfer of electron and lithium ion and lower interface contact resistance [58,59]. As a result, higher capacity and lower polarization potential are demonstrated (Figs. 5c and S4). After 100 cycles at 1 C, the

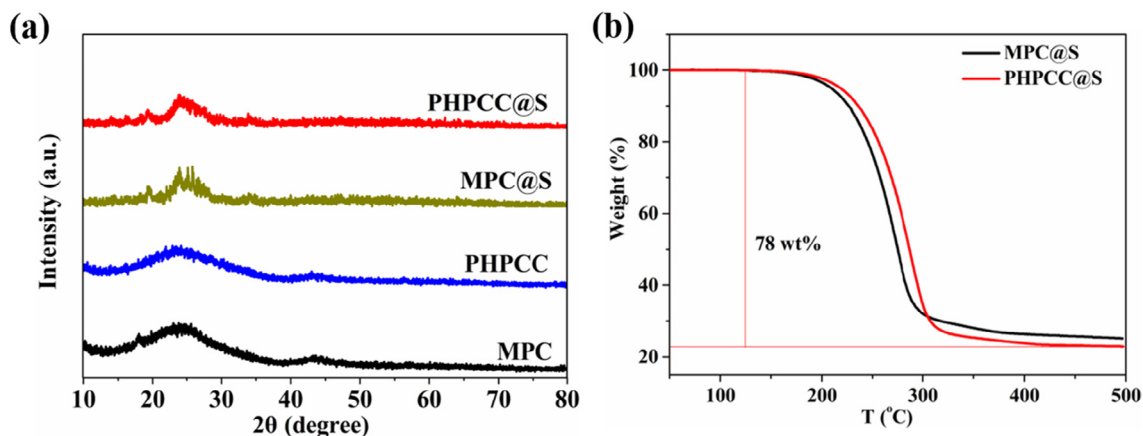
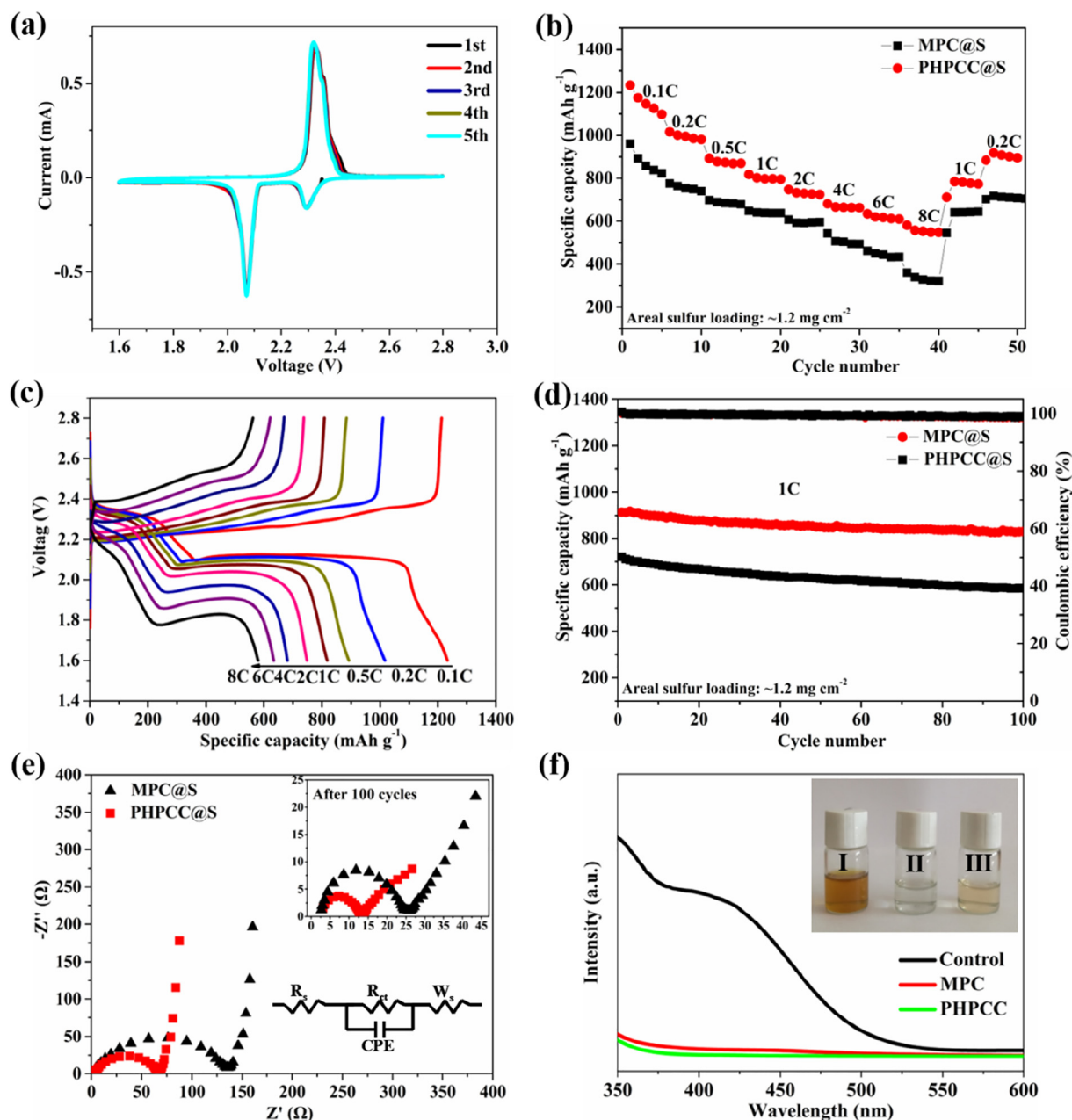


Fig. 4. (a) XRD patterns and (b) TGA curves of MPC@S and PHPCC@S composites.



**Fig. 5.** (a) Cyclic voltammetry (CV) curves of PHPCC@S cathode within the scan range from 1.6 to 2.8 V (vs. Li/Li<sup>+</sup>) at the scan rate of 0.1 mV s<sup>-1</sup>; (b) The rate comparison among MPC@S and PHPCC@S cathodes with sulfur loading of ~1.2 mg cm<sup>-2</sup>; (c) The charge-discharge profiles of PHPCC@S cathode at rates varying from 0.1 to 8 C; (d) Cycling performance comparison of cathodes with sulfur loading of ~1.2 mg cm<sup>-2</sup> at 1 C; (e) Electrochemical impedance spectra (EIS) of the cathodes before cycling and the inset after 100 cycles; (f) UV-vis spectra of the polysulfide solution after exposure to the different adsorbents and the inset photo images of polysulfide solution after exposure to the adsorbents for 8 h (I: contrast; II: PHPCC and III: MPC).

$R_{ct}$  for PHPCC@S cathode (the inset of Fig. 5e) become smaller, which indicates a more stable cathode-electrolyte interface due to the sufficient electrolyte accessibility to the mesopores of the carbon and the well redistribution of the final discharge product Li<sub>2</sub>S on the carbon container, granting fast reaction kinetics. The ability of polar PHPCC toward trapping and adsorbing polysulfides were experimentally proved through ultraviolet visible (UV-vis) method, as shown in Fig. 5f. In the experiments, the equal mass of MPC and PHPCC were immersed into 5 mmol L<sup>-1</sup> Li<sub>2</sub>S<sub>8</sub> solution, respectively. After a long enough adsorption, the coloration of the Li<sub>2</sub>S<sub>8</sub> solutions were recorded. The residual polysulfides concentration after adsorption were measured to evaluate the absorptivity to polysulfides. As displayed in the inset of Fig. 5f, the PHPCC sample shows colorless in contrast to the weak color of MPC and strong color of the pristine Li<sub>2</sub>S<sub>8</sub> solution (control sample),

which strongly demonstrates that the adsorptive ability of the PHPCC is superior to the MPC. In the ultraviolet visible (UV-vis) measurement (Fig. 5f), strong absorbance within the wavelength region of 400–500 nm is clearly observed for the pristine polysulfide solution while quite weak feature of UV-vis adsorption toward polysulfides are indicated for MPC and PHPCC. This implies the strong absorptivity of PHPCC to polysulfides. The residual concentration of the solutions decreased in the following order: Contrast > MPC > PHPCC. And the adsorption efficiency of the MPC and PHPCC is 94% and 98%, respectively. The adsorption capacity of the PHPCC and MPC is 0.079 g Polysulfides/g Adsorbent and 0.076 g/g, respectively, slightly larger than the reported literature [60].

Fig. 6a shows prolonged cyclability of PHPCC@S at high current density of 2 C. The discharge capacity is initial 805 mA h g<sup>-1</sup>. After 400



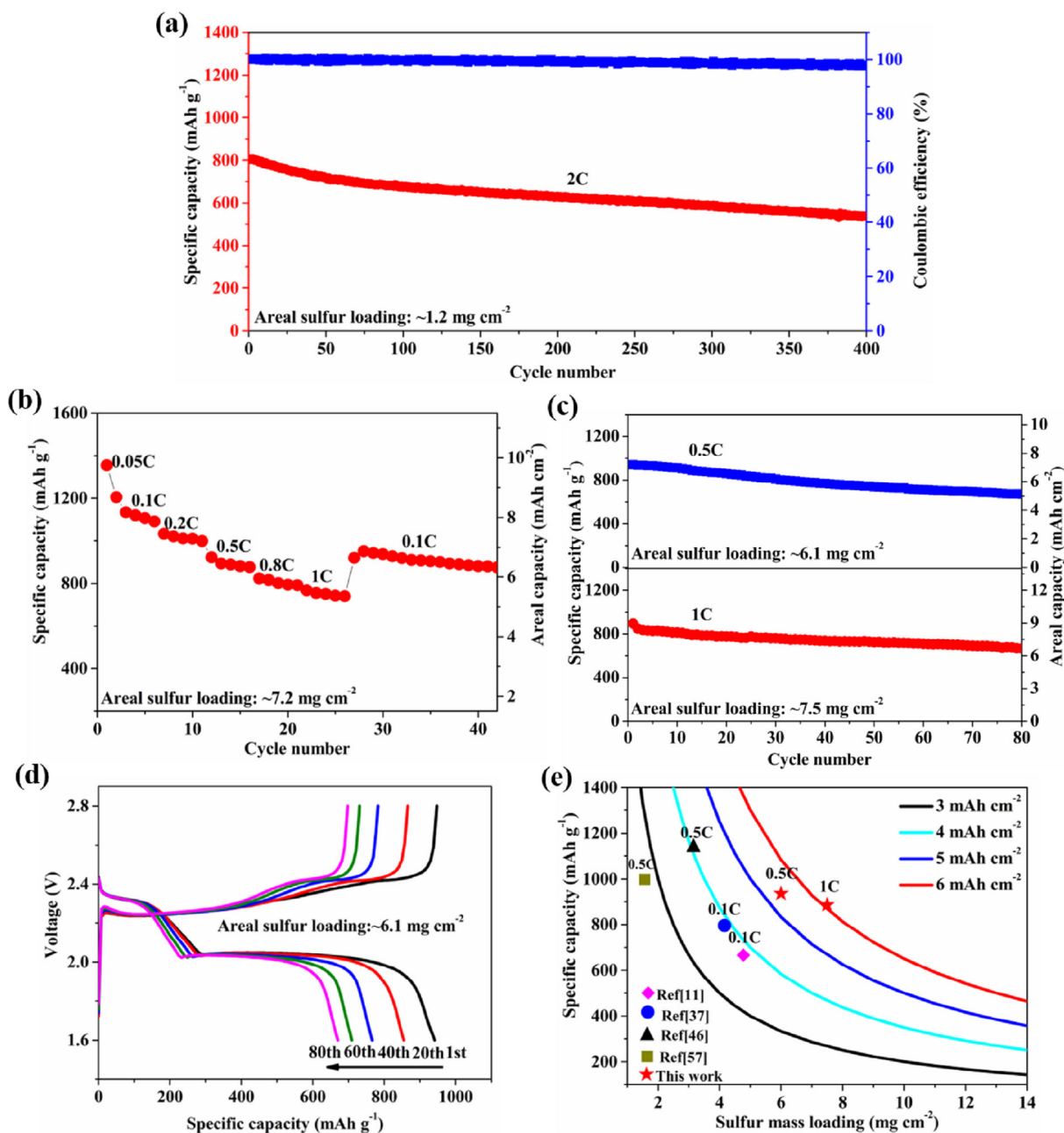


**Fig. 6.** (a) Prolonged cyclability of PHPCC@S cathode with sulfur loading of  $1.2 \text{ mg cm}^{-2}$  at 2 C; (b) Rate performance of PHPCC@S cathode with a high sulfur loading of  $7.2 \text{ mg cm}^{-2}$ ; (c) Cycling performance of PHPCC@S cathode with high sulfur loading at 0.5 C and 1 C; (d) Voltage-capacity profiles with a high sulfur loading at 0.5 C; (e) Comparisons of initially areal capacity between the PHPCC@S cathode in our work and others using nanocomposites matrixes reported in the previous literatures.

cycles, the cathode still remains a reversible capacity of  $536 \text{ mA h g}^{-1}$ , and the capacity decay rate is as low as 0.08% per cycle. Overall, the coulombic efficiency of the PHPCC@S cathode is still above 98% within 400 cycles. The realization of a slow capacity decay rate and high coulombic efficiency suggests that the shuttle effect could be effectively alleviated by the synergetic confinements of the carbon container.

For the commercialization purpose of Li-S battery, the sulfur mass loading above  $4 \text{ mg cm}^{-2}$  and the areal capacity higher than  $4 \text{ mA h cm}^{-2}$  are needed [10–13]. Owing to the large pore volume and surface area, the thickness of loaded sulfur layer is thin enough to be anchored by the polar active sites even under the condition of a high sulfur loading. On the other hand, the hierarchical pores in the carbon framework is helpful for forming interconnected structure, which give an easy access for rapid ion and electron transportation. Moreover, our

carbon container possesses high density of the doped N and S functional sites in the container. The optimized pore structure with high number of polar sites allows efficient chemisorption of polysulfides (Fig. 5f) to weaken the shuttle effect and well redistribute the polysulfides on the pore walls of the matrix without sacrificing the overall conductivity of the carbon framework. Therefore, it is of great necessity to explore whether the PHPCC with large pore container and polar active sites works well under high sulfur loading.

The rate performance of the PHPCC@S cathode from 0.05 to 1 C was carried out under high loading of  $7.2 \text{ mg cm}^{-2}$  (Fig. 6b). It delivers an initial specific discharge capacity of  $1355 \text{ mA h g}^{-1}$  at 0.05 C, corresponding to a high areal capacity of  $9.75 \text{ mA h cm}^{-2}$ . The further cycling at 0.2 C, 0.5 C and 1 C decreases the capacities to be  $1032 \text{ mA h g}^{-1}$  ( $7.4 \text{ mA h cm}^{-2}$ ),  $922 \text{ mA h g}^{-1}$  ( $6.6 \text{ mA h cm}^{-2}$ ) and



767 mA h g<sup>-1</sup> (5.5 mA h cm<sup>-2</sup>), respectively. When the current rate switches to 0.1 C, a reversible areal capacity of 6.8 mA h cm<sup>-2</sup> is obtained, suggesting the good rate performance of the high mass loading cathode. Then, the cells with 7.5 mg cm<sup>-2</sup> sulfur were subjected to 1 C cycling to further verify the cycling stability (Fig. 6c). It presents an initial capacity of 895 mA h g<sup>-1</sup> corresponding to a high areal capacity of 6.7 mA h cm<sup>-2</sup>. After 80 cycles, the cathode remains an areal capacity of approximately 5.0 mA h cm<sup>-2</sup>, corresponding to the retention rate of 75%. In addition, the cell still delivers stable voltage profiles (Fig. 6d) with acceptable polarization potentials (Fig. S7a). The coulombic efficiencies of the cathodes are still above 96% within 80 cycles (Fig. S7b). As reported in the literatures [11,36], most of the cathodes delivered low areal capacity values (below 4 mA h cm<sup>-2</sup>). For a better understanding, the areal capacities estimated from some recent literatures are marked in Fig. 6e. Our work provides initially areal capacity values as high as 6.7 mA h cm<sup>-2</sup> at 0.5 C and 5.7 mA h cm<sup>-2</sup> at 1 C, respectively, which is about 2–5 times higher than the previous reports of nanocomposite matrixes [11,37,42,45,46], even at a high current rate of 1 C.

A proper electrolyte amount and areal loading of the electrode exhibit a trade-off relationship in the high sulfur loading battery. A different electrolyte/sulfur (E/S) ratio was also investigated, and the electrolyte amount can be lowered down to 15  $\mu$ L mg<sup>-1</sup> in the coin cell (Fig. S8a) since the extra electrolyte need to fill in the void space in the coin cell, which still displays more competitive areal capacity than the reported material with 16  $\mu$ L mg<sup>-1</sup> electrolyte [41]. To further decrease the E/S ratio, the pouch cell based on large areal cathode was prepared and assembled. As displayed in Fig. S8b, a pouch cell with sulfur loading of 4 mg cm<sup>-2</sup> and E/S ratio as low as 7  $\mu$ L mg<sup>-1</sup> can also work well and exhibits an initial capacity of 733 mA h g<sup>-1</sup> (2.9 mA h cm<sup>-2</sup>) and a reversible capacity of 528 mA h g<sup>-1</sup> (2.1 mA h cm<sup>-2</sup>) after 30 cycles at 0.2 C, showing the excellent stability. And the initially gravimetric energy density of the cell at 0.2 C is calculated to be 1613 Wh kg<sup>-1</sup> based on the weight of sulfur. In the future, it is also urgent to optimize the whole cell parameters on the premise of high mass loading to promise practical Li/S battery applications.

#### 4. Conclusions

In summary, we fabricate a hierarchical-porous carbon container with large pore volume and polar heteroatoms sites for synergistically confinement of sulfur species, aiming at improving the areal capacity of Li-S batteries for practical application. The as-prepared synergistic carbon container with polar elemental sites provides an affordable space for holding sulfur species, tolerating volume change, providing rapid ion/electron transfer pathway and sufficient electrolyte immersion. Benefiting from these merits, the as-synthesized PHPCC@S cathode with a moderate sulfur loading displays a high rate specific capacity of 581 mA h g<sup>-1</sup> at 8 C and a stable cyclability at 2 C. More importantly, the cathode with an areal sulfur loading as high as 7.2 mg cm<sup>-2</sup> presents a high areal capacity of 9.75 mA h cm<sup>-2</sup> at 0.05 C, and higher rate performance with 5.5 mA h cm<sup>-2</sup> at 1 C. The cathode with 7.5 mg cm<sup>-2</sup> can initially deliver a high areal capacity of 6.7 mA h cm<sup>-2</sup> at 1 C and still retain 5.0 mA h cm<sup>-2</sup> after 80 cycles, corresponding to capacity retention of 75%. Moreover, the container can successfully work in a pouch cell with low E/S ratio. Our PHPCC container shows a significantly practical potential for the fabrication of high areal capacity sulfur cathode.

#### Acknowledgments

This work was in part supported by the International Science and Technology Cooperation Program of China (2015DFR50350), the National Natural Science Foundation of China (No. 51771145), Shaanxi key R & D plan, international scientific and technological cooperation and exchange program (No. 2017KW-020), Shaanxi Natural Science

Basic Research Plan (No. 2017JM5060). The authors are also grateful to the Instrument Analysis Center of Xi'an Jiaotong University for Raman spectroscopy measurements and Dr. Yaning Feng for very helpful suggestions regarding the preparation of mesoporous carbon.

#### Appendix A. Supplementary data

Supplementary data to this article can be found online at <https://doi.org/10.1016/j.cej.2019.02.171>.

#### References

- [1] C. Lin, C. Niu, X. Xu, K. Li, Z. Cai, Y. Zhang, X. Wang, L. Qu, Y. Xu, L. Mai, A facile synthesis of three dimensional graphene sponge composited with sulfur nanoparticles for flexible Li-S cathodes, *Phys. Chem. Chem. Phys.* 18 (2016) 22146–22153.
- [2] J.R. He, Y.F. Chen, P.J. Li, F. Fu, Z.G. Wang, W.L. Zhang, Three-dimensional CNT/graphene-sulfur hybrid sponges with high sulfur loading as superior-capacity cathode for lithium-sulfur batteries, *J. Mater. Chem. A* 3 (2015) 18605–18610.
- [3] X. Chen, Z.B. Xiao, X.T. Ning, Z. Liu, Z. Yang, C. Zou, S. Wang, X.H. Chen, Y. Chen, S.M. Huang, Sulfur-impregnated, sandwich-type, hybrid carbon nanosheets with hierarchical porous structure for high-performance lithium-sulfur batteries, *Adv. Energy Mater.* 4 (2014) 1301988.
- [4] F. Pei, L. Lin, D. Ou, Z. Zheng, S. Mo, X. Fang, N. Zheng, Self-supporting sulfur cathodes enabled by two-dimensional carbon yolk-shell nanosheets for high-energy-density lithium-sulfur batteries, *Nat. Commun.* 8 (2017) 482.
- [5] L.L. Kong, Z. Zhang, Y.Z. Zhang, S. Liu, G.R. Li, X.P. Gao, Porous carbon paper as interlayer to stabilize the lithium anode for lithium-sulfur battery, *ACS Appl. Mater. Interfaces* 8 (2016) 31684–31694.
- [6] C. Hu, H. Chen, Y. Shen, D. Lu, Y. Zhao, A.H. Lu, X. Wu, W. Lu, L. Chen, In situ wrapping of the cathode material in lithium-sulfur batteries, *Nat. Commun.* 8 (2017) 479.
- [7] Y. Hou, J. Li, X. Gao, Z. Wen, C. Yuan, J. Chen, 3D dual-confined sulfur encapsulated in porous carbon nanosheets and wrapped with graphene aerogels as a cathode for advanced lithium sulfur batteries, *Nanoscale* 8 (2016) 8228–8235.
- [8] J. Balach, T. Jaumann, M. Klose, S. Oswald, J. Eckert, L. Giebeler, Functional mesoporous carbon-coated separator for long-life, high-energy lithium-sulfur batteries, *Adv. Funct. Mater.* 25 (2015) 5285–5291.
- [9] W.L. Cai, G.R. Li, K.L. Zhang, G.N. Xiao, C. Wang, K.F. Ye, Z.W. Chen, Y.C. Zhu, Y.T. Qian, Conductive nanocrystalline niobium carbide as high efficiency polysulfides tamer for lithium-sulfur batteries, *Adv. Funct. Mater.* 28 (2018) 1704865.
- [10] G.M. Zhou, L. Li, C.Q. Ma, S.G. Wang, Y. Shi, N. Koratkar, W.C. Ren, F. Li, H.M. Cheng, A graphene foam electrode with high sulfur loading for flexible and high energy Li-S batteries, *Nano Energy* 11 (2015) 356–365.
- [11] T. Xu, J. Song, M.L. Gordin, H. Sohn, Z. Yu, S. Chen, D. Wang, Mesoporous carbon-carbon nanotube-sulfur composite microspheres for high-areal-capacity lithium-sulfur battery cathodes, *ACS Appl. Mater. Interfaces* 5 (2013) 11355–11362.
- [12] J. Wang, S. Cheng, W.F. Li, L.J. Jia, Q.B. Xiao, Y. Hou, Z.Z. Zheng, H.F. Li, S. Zhang, L.S. Zhou, M.N. Liu, H.Z. Lin, Y.G. Zhang, Robust electrical “highway” network for high mass loading sulfur cathode, *Nano Energy* 40 (2017) 390–398.
- [13] H.J. Peng, J.Q. Huang, X.Y. Liu, X.B. Cheng, W.T. Xu, C.Z. Zhao, F. Wei, Q. Zhang, Healing high-loading sulfur electrodes with unprecedented long cycling life: spatial heterogeneity control, *J. Am. Chem. Soc.* 139 (2017) 8458–8466.
- [14] A. Jozwiuk, B.B. Berkes, T. Weiss, H. Sommer, J. Janek, T. Brezesinski, The critical role of lithium nitrate in the gas evolution of lithium-sulfur batteries, *Energy Environ. Sci.* 9 (2016) 2603–2608.
- [15] G. Zheng, Y. Yang, J.J. Cha, S.S. Hong, Y. Cui, Hollow carbon nanofiber-encapsulated sulfur cathodes for high specific capacity rechargeable lithium batteries, *Nano. Lett.* 11 (2011) 4462–4467.
- [16] W. Ai, W.W. Zhou, Z.Z. Du, Y. Chen, Z.P. Sun, C. Wu, C.J. Zou, C.M. Lie, W. Huang, T. Yu, Nitrogen and phosphorus codoped hierarchically porous carbon as an efficient sulfur host for Li-S batteries, *Energy Storage Mater.* 6 (2017) 112–118.
- [17] Z. Wei, S. H. Li, J.J. Cha, G. Zheng, Y. Yang, M.T. McDowell, P.C. Hsu, Y. Cui, Sulfur-TiO<sub>2</sub> yolk-shell nanoarchitecture with internal void space for long-cycle lithium-sulfur batteries, *Nat. Commun.* 4 (2013) 1331.
- [18] Z.W. Seh, Y. Sun, Q. Zhang, Y. Cui, Designing high-energy lithium-sulfur batteries, *Chem. Soc. Rev.* 45 (2016) 5605–5634.
- [19] B. Papandrea, X. Xu, Y.X. Xu, C.Y. Chen, Z.Y. Lin, G.M. Wang, Y.Z. Luo, M. Liu, Y. Huang, L.Q. Mai, X.F. Duan, Three-dimensional graphene framework with ultra-high sulfur content for a robust lithium-sulfur battery, *Nano Res.* 9 (2016) 240–248.
- [20] A. Manthiram, S.H. Chung, C. Zu, Lithium-sulfur batteries: progress and prospects, *Adv. Mater.* 27 (2015) 1980–2006.
- [21] J.J. Cai, C. Wu, Y. Zhu, K.L. Zhang, P.K. Shen, Sulfur impregnated N, P co-doped hierarchical porous carbon as cathode for high performance Li-S batteries, *J. Power Sources* 341 (2017) 165–174.
- [22] Z. Li, Y.M. Huang, L.X. Yuan, Z.X. Hao, Y.H. Huang, Status and prospects in sulfur-carbon composites as cathode materials for rechargeable lithium-sulfur batteries, *Carbon* 92 (2015) 41–63.
- [23] A. Eftekhari, D.W. Kim, Cathode materials for lithium-sulfur batteries: a practical perspective, *J. Mater. Chem. A* 5 (2017) 17734–17776.
- [24] L. Li, L. Chen, S. Mukherjee, J. Gao, H. Sun, Z.B. Liu, X.L. Ma, T. Gupta, C.V. Singh, W.C. Ren, H.M. Cheng, N. Koratkar, Phosphorene as a polysulfide immobilizer and

- catalyst in high-performance lithium-sulfur batteries, *Adv. Mater.* 29 (2017) 1602734.
- [25] X. Liu, J.Q. Huang, Q. Zhang, L. Mai, Nanostructured metal oxides and sulfides for lithium-sulfur batteries, *Adv. Mater.* 29 (2017) 1601759.
- [26] H.L. Wu, Y. Li, J. Ren, D.W. Rao, Q.J. Zheng, L. Zhou, D.M. Lin, CNT-assembled dodecahedra core@nickel hydroxide nanosheet shell enabled sulfur cathode for high-performance lithium-sulfur batteries, *Nano Energy* 55 (2019) 82–92.
- [27] H.L. Wu, L. Xia, J. Ren, Q.J. Zheng, C.G. Xu, D.M. Lin, A high-efficiency N/P co-doped graphene/CNT@porous carbon hybrid matrix as a cathode host for high performance lithium-sulfur batteries, *J. Mater. Chem. A* 5 (2017) 20458–20472.
- [28] J. Ren, Y.B. Zhou, L. Xia, Q.J. Zheng, J. Liao, E. Long, F.Y. Xie, C.G. Xu, D.M. Lin, Rational design of a multidimensional N-doped porous carbon/MoS<sub>2</sub>/CNT nano-architecture hybrid for high performance lithium-sulfur batteries, *J. Mater. Chem. A* 6 (2018) 13835–13847.
- [29] K. Sun, C.A. Cama, J. Huang, Q. Zhang, S. Hwang, D. Su, A.C. Marschilok, K.J. Takeuchi, E.S. Takeuchi, H. Gan, Effect of carbon and binder on high sulfur loading electrode for Li-S battery technology, *Electrochim. Acta* 235 (2017) 399–408.
- [30] S. Rehman, X.X. Gu, K. Khan, N. Mahmood, W.L. Yang, X.X. Huang, S.J. Guo, Y.L. Hou, 3D vertically aligned and interconnected porous carbon nanosheets as sulfur immobilizers for high performance lithium-sulfur batteries, *Adv. Energy Mater.* 6 (2016) 1502518.
- [31] L. Qie, A. Manthiram, A facile layer-by-layer approach for high-areal-capacity sulfur cathodes, *Adv. Mater.* 27 (2015) 1694–1700.
- [32] M.A. Pope, I.A. Aksay, Structural design of cathodes for Li-S batteries, *Adv. Energy Mater.* 5 (2015) 1500124.
- [33] F. Liu, Q. Xiao, H.B. Wu, F. Sun, X. Liu, F. Li, Z. Le, L. Shen, G. Wang, M. Cai, Y. Lu, Regenerative polysulfide-scavenging layers enabling lithium-sulfur batteries with high energy density and prolonged cycling life, *ACS Nano* 11 (2017) 2697–2705.
- [34] M. Li, R. Carter, A. Douglas, L. Oakes, C.L. Pint, Sulfur vapor-infiltrated 3D carbon nanotube foam for binder-free high areal capacity lithium-sulfur battery composite cathodes, *ACS Nano* 11 (2017) 4877–4884.
- [35] G. Hu, C. Xu, Z. Sun, S. Wang, H.M. Cheng, F. Li, W. Ren, 3D graphene-foam-reduced-graphene-oxide hybrid nested hierarchical networks for high-performance Li-S batteries, *Adv. Mater.* 28 (2016) 1603–1609.
- [36] S. Dorfler, M. Hagen, H. Althues, J. Tubke, S. Kaskel, M.J. Hoffmann, High capacity vertical aligned carbon nanotube/sulfur composite cathodes for lithium-sulfur batteries, *Chem. Commun. (Camb)* 48 (2012) 4097–4099.
- [37] J.X. Song, T. Xu, M.L. Gordin, P.Y. Zhu, D.P. Lv, Y.B. Jiang, Y.S. Chen, Y.H. Duan, D.H. Wang, Nitrogen-doped mesoporous carbon promoted chemical adsorption of sulfur and fabrication of high-areal-capacity sulfur cathode with exceptional cycling stability for lithium-sulfur batteries, *Adv. Funct. Mater.* 24 (2014) 1243–1250.
- [38] A. Schneider, C. Suchowski, H. Sommer, J. Janek, T. Brezesinski, Free-standing and binder-free highly N-doped carbon/sulfur cathodes with tailorable loading for high-areal-capacity lithium-sulfur batteries, *J. Mater. Chem. A* 3 (2015) 20482–20486.
- [39] L. Qie, C.X. Zu, A. Manthiram, A high energy lithium-sulfur battery with ultrahigh-loading lithium polysulfide cathode and its failure mechanism, *Adv. Energy Mater.* 6 (2016) 1502459.
- [40] D.P. Lv, J.M. Zheng, Q.Y. Li, X. Xie, S. Ferrara, Z.M. Nie, L.B. Mehdii, N.D. Browning, J.G. Zhang, G.L. Graff, J. Liu, J. Xiao, High energy density lithium-sulfur batteries: challenges of thick sulfur cathodes, *Adv. Energy Mater.* 5 (2015) 1402290.
- [41] J. Gao, H.D. Abruna, Key parameters governing the energy density of rechargeable Li/S batteries, *J. Phys. Chem. Lett.* 5 (2014) 882–885.
- [42] T. Chen, B. Cheng, G. Zhu, R. Chen, Y. Hu, L. Ma, H. Lv, Y. Wang, J. Liang, Z. Tie, Z. Jin, J. Liu, Highly efficient retention of polysulfides in “Sea Urchin”-like carbon nanotube/nanopolyhedra superstructures as cathode material for ultralong-life lithium-sulfur batteries, *Nano Lett.* 17 (2017) 437–444.
- [43] D.S. Jung, T.H. Hwang, J.H. Lee, H.Y. Koo, R.A. Shakoor, R. Kahraman, Y.N. Jo, M.S. Park, J.W. Choi, Hierarchical porous carbon by ultrasonic spray pyrolysis yields stable cycling in lithium-sulfur battery, *Nano Lett.* 14 (2014) 4418–4425.
- [44] Z.J. Guo, B. Zhang, D.J. Li, T. Zhao, P.R. Coxon, C.J. Harris, R. Hao, Y.J. Liu, K. Xi, X.F. Li, A mixed microporous/low-range mesoporous composite with high sulfur loading from hierarchically-structured carbon for lithium sulfur batteries, *Electrochim. Acta* 230 (2017) 181–188.
- [45] Z. Li, Y. Jiang, L. Yuan, Z. Yi, C. Wu, Y. Liu, P. Strasser, Y. Huang, A highly ordered meso@microporous carbon-supported sulfur@smaller sulfur core-shell structured cathode for Li-S batteries, *ACS Nano* 8 (2014) 9295–9303.
- [46] Q. Pang, J. Tang, H. Huang, X. Liang, C. Hart, K.C. Tam, L.F. Nazar, A nitrogen and sulfur dual-doped carbon derived from polyrhodanine@cellulose for advanced lithium-sulfur batteries, *Adv. Mater.* 27 (2015) 6021–6028.
- [47] G.M. Zhou, Y.B. Zhao, A. Manthiram, Dual-confined flexible sulfur cathodes encapsulated in nitrogen-doped double-shelled hollow carbon spheres and wrapped with graphene for Li-S batteries, *Adv. Energy Mater.* 5 (2015) 1402263.
- [48] J. Wang, S. Cheng, W.F. Li, S. Zhang, H.F. Li, Z.Z. Zheng, F.J. Li, L.Y. Shi, H.Z. Lin, Y.G. Zhang, Simultaneous optimization of surface chemistry and pore morphology of 3D graphene-sulfur cathode via multi-ion modulation, *J. Power Sources* 321 (2016) 193–200.
- [49] S. Niu, W. Lv, G. Zhou, Y. He, B. Li, Q.H. Yang, F. Kang, N and S co-doped porous carbon spheres prepared using L-cysteine as a dual functional agent for high-performance lithium-sulfur batteries, *Chem. Commun. (Camb)* 51 (2015) 17720–17723.
- [50] J. Yang, J. Xie, X.Y. Zhou, Y.L. Zou, J.J. Tang, S.C. Wang, F. Chen, L.Y. Wang, Functionalized N-doped porous carbon nanofiber webs for a lithium-sulfur battery with high capacity and rate performance, *J. Phys. Chem. C* 118 (2014) 1800–1807.
- [51] Q. Wang, H. Zhong, M. Jiang, Q.C. Liao, J. Yang, X.Y. Zhou, J.J. Tang, Recycling antibiotic bacterial residues for application in high-performance lithium-sulfur batteries, *ChemElectroChem* 5 (2018) 2235–2241.
- [52] M. Li, Y.N. Zhang, X.L. Wang, W. Ahn, G.P. Jiang, K. Feng, G. Lui, Z.W. Chen, Gas pickering emulsion templated hollow carbon for high rate performance lithium sulfur batteries, *Adv. Funct. Mater.* 26 (2016) 8408–8417.
- [53] J. Schuster, G. He, B. Mandlmeier, T. Yim, K.T. Lee, T. Bein, L.F. Nazar, Spherical ordered mesoporous carbon nanoparticles with high porosity for lithium-sulfur batteries, *Angew. Chem. Int. Ed. Engl.* 51 (2012) 3591–3595.
- [54] J. Balach, T. Jaumann, M. Klose, S. Oswald, J. Eckert, L. Giebeler, Mesoporous carbon interlayers with tailored pore volume as polysulfide reservoir for high-energy lithium-sulfur batteries, *J. Phys. Chem. C* 119 (2015) 4580–4587.
- [55] K.K. Beltrame, A.L. Cazetta, P.S.C. de Souza, L. Spessato, T.L. Silva, V.C. Almeida, Adsorption of caffeine on mesoporous activated carbon fibers prepared from pineapple plant leaves, *Ecotoxicol. Environ. Saf.* 147 (2018) 64–71.
- [56] H.T. Liu, Y.Q. Liu, D.B. Zhu, Chemical doping of graphene, *J. Mater. Chem.* 21 (2011) 3335–3345.
- [57] S. Xin, Y. You, H.Q. Li, W. Zhou, Y. Li, L. Xue, H.P. Cong, Graphene sandwiched by sulfur-confined mesoporous carbon nanosheets: a kinetically stable cathode for Li-S batteries, *ACS Appl. Mater. Interfaces* 8 (2016) 33704–33711.
- [58] J. Zhang, C.Y. You, W.H. Zhang, J. Wang, S.H. Guo, R. Yang, Y.H. Xu, Conductive bridging effect of TiN nanoparticles on the electrochemical performance of TiN@CNT-S composite cathode, *Electrochim. Acta* 250 (2017) 159–166.
- [59] F. Wu, J. Qian, R.J. Chen, T. Zhao, R. Xu, Y.S. Ye, W.H. Li, L. Li, J. Lu, K. Amine, Sulfur cathode based on layered carbon matrix for high-performance Li-S batteries, *Nano Energy* 12 (2015) 742–749.
- [60] A. Schneider, J. Janek, T. Brezesinski, Improving the capacity of lithium-sulfur batteries by tailoring the polysulfide adsorption efficiency of hierarchical oxygen/nitrogen-functionalized carbon host materials, *Phys. Chem. Chem. Phys.* 19 (2017) 8349–8355.